Regular Article

PHYSICAL CHEMISTRY RESEARCH
Published by the
Iranian Chemical Society
www.physchemres.org
info@physchemres.org

Phys. Chem. Res., Vol. 10, No. 1, 89-104, March 2022
DOI: 10.22036/pcr.2021.292510.1930

The Effects of the Ionic Field Strength of Be^{2+}, Mg^{2+}, and Ca^{2+} and a Static Electric Field (SEF) on the Interaction Between Prothionamide and $B_{12}P_{12}$ Nanocage: A DFT and TD-DFT Study

M. Rezaei-Sameti* and H. Khani
Department of Applied Chemistry, Faculty of Science, Malayer University, Malayer, Iran
(Received 29June 2021, Accepted 1 September 2021)

In the present study, the potential of $B_{12}P_{12}$ nanocage in detecting and delivering prothionamide (PA) in the presence of a static electric field (SEF = 0.005 to SEF = 0.075 a.u.) and Be^{2+}, Mg^{2+}, and Ca^{2+} ions, encapsulated inside the $B_{12}P_{12}$ nanocage, was investigated at cam-B3LYP/6-31G(d,p) level of theory using the Gaussian 09 package program. The electrical, quantum, and thermodynamic properties, the quantum theory of atoms in molecules (QTAIM), UV-Vis, IR spectra, and reduced density gradient (RDG) of all systems were calculated. The results of AIM, RDG, localized-orbital locator (LOL), and electron localization function (ELF) analyses showed that there was a sigma and electrostatic bond between PA and nanocage. The Be^{2+} ion had the greatest effect on the electrical behavior of nanocage and increased the conductivity, activity, and electron affinity of nanocage, which together play an important role in the interaction of nanocage with drugs. The E_{ads}, ΔG, and ΔH values of PA adsorption on the surface of the $Be^{2+}@B_{12}P_{12}$ nanocage were more than those in other models. The calculation results showed that the SEF did not play a significant role in the conductivity properties of nanocage and the development of a suitable drug sensor.

Keywords: Encapsulated ions, SEF, $B_{12}P_{12}$, Prothionamide, DFT

INTRODUCTION

In recent years, scientific advances in the production of nanoparticles have led to extensive experimental and theoretical research aimed at developing and manufacturing various nanoparticles. Among the nanomaterials, the nanocages of the third and fifth groups of the periodic table (X_nY_n: X = B, Al, and Y = N, P: $(AlN)_n$ $(AlP)_n$, $(BN)_n$, and $(BP)_n$) have received more attention in recent years due to their unique physical and chemical properties and high surface-to-volume ratio. Also, they are considered promising materials for use in optoelectronic and microelectronic devices designed to work under harsh conditions, such as extreme temperatures, and aggressive environments [1-10]. Theoretical studies on several $(XY)_n$ nanocages have shown that the fullerene-like cage with n = 12 is the most stable nanocage among other nanocages with different sizes [11-14]. The nanocages belonging to these groups have remarkable electronic and semiconducting properties [15-20]. These spherical nanocages have been synthesized experimentally and detected using time-of-flight mass spectrometry [21-22].

The effects of guanine, oxygen, furan, chlorine (Cl_2), and dimethyl ether (DME) adsorption on four $X_{12}Y_{12}$ nanocages ($Al_{12}N_{12}$, $Al_{12}P_{12}$, $B_{12}N_{12}$, and $B_{12}P_{12}$) were investigated [23-30], and the results confirmed that the electronic properties of nanocages altered significantly from their original states during the adsorption process.

Boron phosphide (BP) is a polar and semiconductor compound. Due to its special features and capabilities, it can be used in electronic and microelectronic devices designed to work in harsh conditions and extreme temperatures [31]. Recently, some studies have investigated the adsorption of carbon monoxide (CO), nitrogen monoxide (NO), phenol,

*Corresponding author. E-mail: mrsameti@malayeru.ac.ir

phosgene, and H_2 on AlN, BN, and BP nanomaterials [32-36]. The results of these studies have shown that the adsorption process at all adsorption models was exothermic and increased the electrical conductivity and properties of the systems. Sajida Munsif *et al.* found that doping of alkali metal on aluminum phosphide and BP nanocages significantly altered the nonlinear optical response of nanocages and the hyperpolarizability properties of the studied complex [37]. Other computational studies have indicated that the decoration of nickel and encapsulation of different halide ions can significantly enhance the adsorption capacity of BP nanocage for H_2/H compounds and cell voltage of Na-ion battery [38-41]. In a computational study, Razavi *et al.* showed that the $B_{14}P_{14}$ nanocage, which is used as the anode in metal-ion batteries, had a higher potential than $Si_{14}Ge_{14}$ and that the K-ion battery had higher potential and cell voltage than Li-ion and Na-ion batteries [42]. Rad *et al.* reported that the adsorption of acetylene (ethylene) molecule on pristine $B_{12}P_{12}$ nanocage was weakly physisorbed and that its adsorption was significantly improved by the decoration of Ni atom [43]. In a theoretical study, Hojatkashani showed that the capability of $B_{12}P_{12}$ nanocage to adsorb CO molecule in the presence of Al and N atoms was 1.7% more than that of pristine models and that the interaction between CO and $B_{12}P_{12}$ nanocage was indicative of a van der Waals type interaction [44]. Kian *et al.* found that the adsorption of Aromasin (AMS) on the $B_{12}N_{12}$ surface was more favorable than on the $B_{12}P_{12}$ surface; thus, they concluded that $B_{12}N_{12}$ nanocages could function as a drug delivery carrier in the treatment of postmenopausal patients with advanced breast cancer [45]. The results of another computational study confirmed that the adsorption of OF_2 on the SH-functionalized $B_{24}P_{24}$ nanocage surface was energetically more favorable than that on the $B_{24}N_{24}$ nanocage surface [46].

Soltani *et al.* found that the energy gap of the $B_{12}P_{12}$ nanocage significantly reduced compared to that of the $B_{12}N_{12}$ nanocage upon the adsorption of OCN^-, leading to an increase in the electrical conductance of $B_{12}P_{12}$ nanocage [47]. In another study, it was found that the adsorption and deformation energy of pyrazinamide (PYR) on Ti-doped BP nanocage increased significantly compared to the original values [48]. The calculation of thermodynamic parameters revealed that the adsorption of PYR on the surface of the doped-$B_{12}P_{12}$ nanocage was more favorable than that of the pristine model.

The aim of this work was to investigate the effects of the ionic field strength of Be^{2+}, Mg^{2+}, and Ca^{2+} and a static electric field (SEF) on the interaction between prothionamide (PA) and BP nanocage ($B_{12}P_{12}$). The results of this study can be used to facilitate the development of drug sensors or drug delivery in biological systems.

COMPUTATIONAL DETAILS

In this study, the adsorption of PA from S, NH_2, and N (pyridine) sites on the surface of pristine and encapsulated Be^{2+}, Mg^{2+}, and Ca^{2+} ions into the $B_{12}P_{12}$ nanocage, were investigated in the absence and presence of a SEF (0.005, 0.01, 0.02, 0.03, 0.05, and 0.075 a.u.). For simplicity, the capital letters A, B, C, and D are used to show pristine and encapsulated Be^{2+}, Mg^{2+}, and Ca^{2+} ions into the $B_{12}P_{12}$ nanocage, respectively, and the small letters a, b, and c are used to denote the adsorption sites of S, NH_2, and N(pyridine) for PA, respectively (Fig. 1).

All selected stable models were optimized at the cam-B3LYP level of theory with the 6-31G(d,p) basis set using the Gaussian 09 package program [49]. The imaginary vibrational frequency was not shown in any of the adsorption models. The optimization criteria in all studied models for maximum, root-mean-square (RMS), maximum displacement, and RMS displacement forces were set at

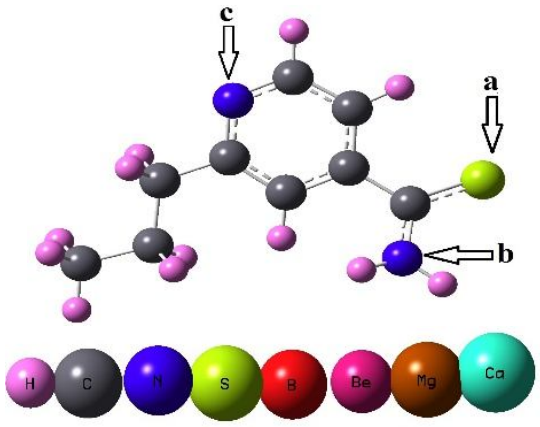

Fig. 1. 2D images of prothionamide (PA) adsorption sites.

0.0004 Hartree/Bohr, 0.0003, 0.0015Bohr, and 0.0011, respectively. From the optimized structures, the adsorption energy (E_{ads}) and thermodynamic parameters (ΔH and ΔG) were calculated using Eqs. (1) and (2).

$$E_{ads} = E_{PA/B_{12}P_{12}} - (E_{B_{12}P_{12}} + E_{PA}) + E_{BSSE} \quad (1)$$

$$\Delta M = M_{PA/B_{12}P_{12}} - (M_{B_{12}P_{12}} + M_{PA}) \qquad M : H, and\ G \quad (2)$$

where $E_{PA/B_{12}P_{12}}$, $E_{B_{12}P_{12}}$, and E_{PA} are the total energy of the $PA/B_{12}P_{12}$ complex, $B_{12}P_{12}$ nanocage, and PA, respectively. The basis set superposition error (BSSE) was found to vary between 0.013 and 0.05 kcal mol^{-1}. The calculated thermodynamic parameters in the gas and solution phases are listed in Table 1. In addition, the adsorption energy of all models in the absence and presence of a SEF are given in Tables 1 and 2.

The quantum properties, such as the energy gap in the absence and presence of a SEF, the global hardness (η), chemical potential (μ), Fermi energy (E_{FL}), electron affinity (ω), and total charge transfer properties (ΔN) [50-55], were calculated for all adsorption models from the HOMO (the highest occupied molecular orbital) and LUMO (the lowest unoccupied molecular orbital) energies, and the results are listed in Tables 3 and 4. The quantum theory of atoms in molecules (QTAIM) parameters, reduced density gradient (RDG), and time-dependent density-functional theory (TD-

Table 1. The Bond Length Between PA and Nanocage (Å), Adsorption Energy (kcal mol^{-1}), NBO Charge Density of Drug (e), Thermodynamic Parameters (kcal mol^{-1}), Gibbs Free Energy in Water, and Ethanol Solvent (kcal mol^{-1}) of $B_{12}P_{12}$/PA Complex for A-a to D-c Models

	$d_{-nano/PA}$	E_{ads}	$\rho_{(NBO)}$	ΔG	ΔH	$\Delta\Delta G_{(W)}$	$\Delta\Delta G_{(Et)}$
A-a	1.986	-12.96	0.67	-0.34	-11.63	0.45	0.46
B-a	1.887	-118.31	0.91	-102.19	-112.79	114.79	114.67
C-a	1.936	-54.63	0.85	-40.14	-53.27	61.12	60.62
D-a	1.940	-53.93	0.84	-40.30	-52.54	61.68	61.15
A-b	1.885	-12.83	0.64	-0.99	-11.52	63.32	23.92
B-b	1.785	-75.61	0.66	-61.18	-70.13	73.77	73.61
C-b	1.820	-21.75	0.52	-10.48	-20.73	31.41	30.89
D-b	1.842	-17.13	0.41	-5.29	-16.49	24.31	23.86
A-c	1.627	-21.02	0.45	-5.26	-18.96	3.56	3.62
B-c	1.533	-129.53	0.78	-112.49	-123.39	125.19	125.06
C-c	1.574	-64.70	0.46	-48.53	-62.68	69.86	69.35
D-c	1.578	-64.07	0.64	-48.54	-61.98	70.24	69.70

Table 2. The Adsorption Energy (kcal mol^{-1}) of $B_{12}P_{12}$/PA Complex for A-a to D-a ($SEF_{Z+0.02}$, $SEF_{Z+0.03}$, $SEFz_{+0.05}$, $SEF_{Z+0.075}$ (a.u.))

	E_{ads} (kcal mol^{-1})						
	Z+0.00	Z+0.005	Z+0.01	Z+0.02	Z+0.03	Z+0.05	Z+0.075
A-a	-12.96	-13.95	-14.69	-15.44	-15.20	-11.52	-3.32
B-a	-118.31	-124.16	-129.65	-139.57	-148.05	-156.54	-140.07
C-a	-54.63	-55.75	-56.61	-57.52	-57.32	-53.32	-43.04
D-a	-53.93	-54.88	-55.60	-56.33	-56.12	-52.83	-46.00

Table 3. The Quantum Properties of $B_{12}P_{12}$, Be^{2+}@ $B_{12}P_{12}$, Mg^{2+}@$B_{12}P_{12}$, Ca^{2+}@$B_{12}P_{12}$, PA, and $B_{12}P_{12}$/PA Complex for A-a to D-c Models

	E_g (eV)	η (eV)	ω (eV)	ΔN
A	3.94	1.97	6.60	2.59
B	1.76	0.88	91.64	14.43
C	2.81	1.41	52.23	8.62
D	2.48	1.24	39.61	6.75
A-a	2.72	1.36	7.60	3.52
B-a	2.38	1.19	48.19	9.00
C-a	1.94	0.97	58.53	10.97
D-a	2.52	1.26	42.12	8.17
A-b	2.73	1.37	7.60	3.33
B-b	2.06	1.03	53.24	10.16
C-b	1.85	0.93	58.89	11.27
D-b	1.60	0.80	62.88	12.56
A-c	2.52	1.26	8.28	3.63
B-c	1.48	0.74	70.43	13.79
C-c	1.03	0.51	100.26	19.75
D-c	1.60	0.80	59.70	12.20
$Drug_{(PA)}$	3.91	1.95	14.85	2.00

$E_g = E_{LUMO} - E_{HOMO}$; $\eta = (E_{LUMO} - E_{HOMO})/2$; $\Delta N = -\mu/\eta$, $\omega = \mu^2/\eta$)) [50-54].

DFT) parameters were also calculated.

RESULTS and DISCUSSION

Structural and Electrical Properties and Adsorption Energy

The optimized and stable structures of all adsorption models are shown in Fig. 2. Based on Table 1, the bond length between the PA and $B_{12}P_{12}$ nanocage varied from 1.533 to 1.986Å. The lowest and highest bond lengths were related to the B–c and B–b models respectively (see Table S4).

Comparison results indicated that the bond length between PA and $B_{12}P_{12}$ nanocage was dependent on two parameters: 1) the orientation of PA adsorption; in this state, the order of adsorption distance was a (from the S site) > b (from the NH_2 site) > c (from the N site); 2) the encapsulation of Be^{2+}, Mg^{2+}, and Ca^{2+} ions inside the $B_{12}P_{12}$ nanocage; in this state, the order of adsorption distance was A (pristine) > D (Ca^{2+} decorated) > C (Mg^{2+} decorated) > B (Be^{2+} decorated). Table 1 shows that upon the encapsulation of Be^{2+}, Mg^{2+}, and Ca^{2+} ions into the $B_{12}P_{12}$ nanocage, the adsorption energy, natural bond orbital charge ($\rho_{(NBO)}$), and thermodynamic parameters of PA/$B_{12}P_{12}$ nanocage complexes changed significantly. Interestingly, with the introduction of Be^{2+} ion into the nanocage, the $\rho_{(NBO)}$ of PA changed more than that of Mg^{2+} and Ca^{2+} ions. Therefore, it can be stated that the effect of the Be^{2+} ion field on the electrical structure of PA/$B_{12}P_{12}$ nanocage complexes was more than that of other ions. This, in turn, leads to a significant increase in the adsorption energy, enthalpy, and Gibbs free energy of adsorption compared to other states.

The adsorption energy and thermodynamic parameters of PA/$B_{12}P_{12}$ nanocage complexes changed according to the adsorption sites and encapsulation of ions into the nanocage as follows: c (from the N site) > a (from the S site) > b (from the NH_2 site) and B (Be^{2+} decorate) > C (Mg^{2+} decorate) > D (Ca^{2+} decorate) > A (pristine), respectively. The adsorption energy and thermodynamic parameter for all

Table 4. The Quantum Properties of PA/$B_{12}P_{12}$ Complex for A-a to D-c Models in the Presence of a Static Electric Field ($SEF_{Z+0.005}$, $SEF_{Z+0.01}$, $SEF_{Z+0.02}$, $SEF_{Z+0.03}$ (a.u.))

Model	E_{HOMO} (eV)					E_{LUMO} (eV)					E_{gap} (eV)				
	Z+0.0	Z+0.005	Z+0.01	Z+0.02	Z+0.03	Z+0.0	Z+0.005	Z+0.01	Z+0.02	Z+0.03	Z+0.0	Z+0.005	Z+0.01	Z+0.02	Z+0.03
A-a	-5.90	-5.92	-5.92	-5.72	-5.46	-3.19	-3.19	-3.20	-3.23	-3.28	2.72	2.73	2.72	2.49	2.19
B-a	-11.9	-11.92	-11.95	-12.00	-11.76	-9.52	-9.48	-9.45	-9.45	-9.52	2.38	2.40	2.49	2.55	2.24
C-a	-11.64	-11.66	-11.68	-11.72	-11.78	-9.7	-9.71	-9.75	-9.88	-10.08	1.94	1.95	1.93	1.84	1.70
D-a	-11.57	-11.59	-11.61	-11.66	-11.72	-9.05	-9.07	-9.11	-9.30	-9.57	2.52	2.52	2.50	2.36	2.16

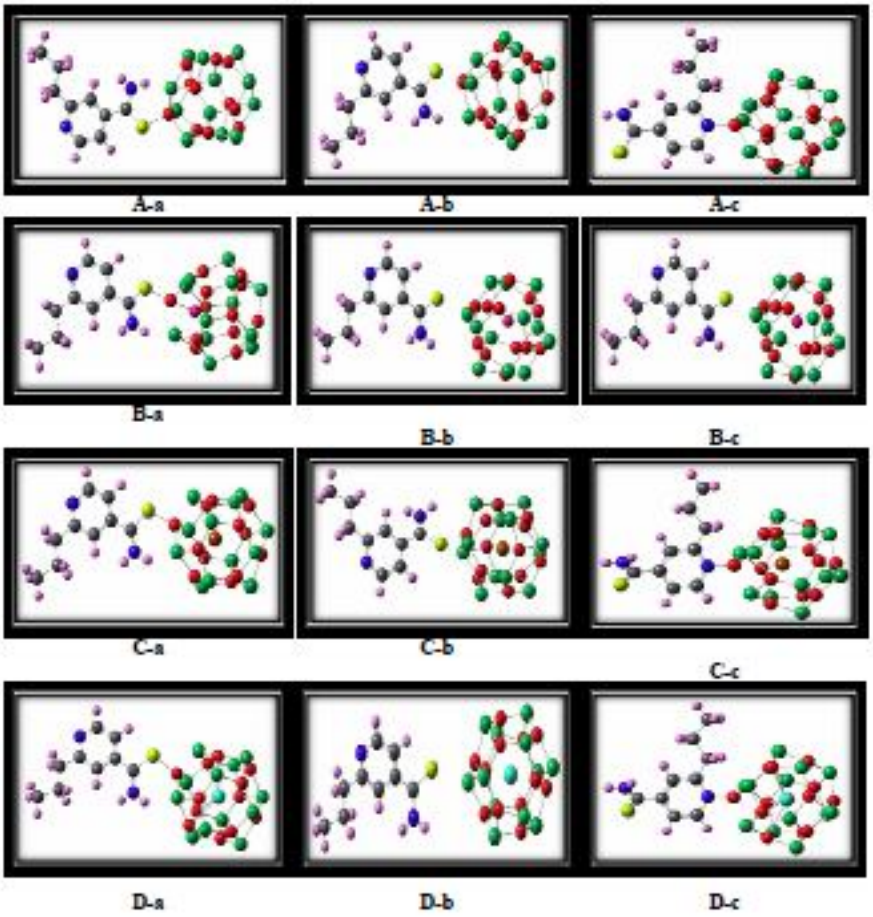

Fig. 2. 2D images of prothionamide (PA) adsorption on the surface of pristine and encapsulated Be^{2+}, Mg^{2+}, and Ca^{2+} ions into the $B_{12}P_{12}$ nanocage (A-a to D-c models).

adsorption models were negative, and all adsorption processes were exothermic and spontaneous. By introducing Be^{2+} ion into the nanocage, the electrostatic field of the system increased significantly due to the high ratio of charge to the surface of the ion. This plays an important role in the binding of PA to the nanocage surface and strengthens the bond between them. The results in Table 1 indicate that the structural and electrical properties of the $PA/B_{12}P_{12}$ nanocage complex were in good agreement with its adsorption energy and thermodynamic parameters. To investigate the adsorption process in water and ethanol solution, the Gibbs free energy ($\Delta\Delta G_{(sol)} = \Delta G_{(sol)\ PA/B12P12} - \Delta G_{(sol)\ (PA} - \Delta G_{(sol)\ (B12P12)}$) of systems were calculated using the polarizable continuum model (PCM) [52], and the results are presented in Table 1. Given that most drug delivery processes take place in solution systems, such as water or ethanol, in the present study, the effects of both water and ethanol solvents on the process of drug uptake and release into the target cells were investigated. The results showed that the value of Gibbs free energy was positive for all models, which indicates that the drug (PA) in solution easily separated from the nanoparticles and attached to the target cell. This highlights the useful and effective therapeutic properties of PA in target cells.

It is noteworthy that the Be^{2+} ion encapsulated into the nanocage played an important role not only in the binding of the drug to the nano in the gas phase but also in the separation of the drug in water and ethanol solution.

Furthermore, it was found that the Be^{2+} ion encapsulated into the nanocage was much more efficient than the other ions in PA delivery. The value of Gibbs free energy in the studied systems varied as follows: in the [c] adsorption site, B-c (w = 125.19, Et = 125.06 kcal mol^{-1}) > D-c (w = 70.24, Et = 69.70 kcal mol^{-1}) > C-c (w = 69.86, Et = 69.35 kcal mol^{-1}) > A-c(w = 3.56, Et = 3.62 kcal mol^{-1}); in the [a] adsorption site, B-a (w = 114.79, Et = 114.67 kcal mol^{-1}) > D-a (w = 61.68, Et = 61.15 kcal mol^{-1}) > C-a (w = 61.12, Et = 60.62 kcal mol^{-1}) > A-a (w = 0.45, Et = 0.46 kcal mol^{-1}); in the [b] adsorption site: B-b (w = 73.77, Et = 73.61 kcal mol^{-1}) > A-b (w = 63.32, Et = 23.92 kcal mol^{-1}) > C-b (w = 31.41, Et = 30.89 kcal mol^{-1}) > D-b (w = 24.31, Et = 23.86 kcal mol^{-1}). The results demonstrated that the dissociation of PA in the presence of water or ethanol solvent was more favorable at the [c] adsorption site than at the [a] and [b] adsorption sites. Moreover, the dissociation of PA from the surface of nanocage and adsorption of it on the surface of the target cells was more favorable at the [c] site than at the other sites. This property of PA at this site (*i.e.*, c) shows that it is a suitable candidate for drug delivery in biological systems.

To understand the effects of a SEF on the adsorption of PA on the surface of nanocage, the 0.005, 0.01, 0.02, 0.03, 0.05, 0.075 (au, 1 a.u. = 514.224 V nm^{-1}) field strength was applied from the z-axis of nanocage in the [a] site of the drug complex, and the calculated results are presented in Table 2.

According to the results in Table 2, it was found that the adsorption process at the A-a, B-a, C-a, and D-a models was exothermic. It is interesting to note that the adsorption of PA drug was more favorable in the presence of the Be^{2+} ion (B-a model) than other models and that more energy was released during the adsorption process at this model compared to other models. A close inspection of the results indicated that the adsorption energy increased in the B-a model when the SEF strength was increased from 0 to 0.05 (a.u.). However, the adsorption energy decreased when the SEF strength was increased to 0.075 (a.u.). Thus, it can be concluded that the Z + 0.05 (a.u.) is the most appropriate SEF strength for adsorbing PA on the surface of the Be^{2+}@B12P12 nanocage.

Also, in the pristine $B_{12}P_{12}$ (A-a model), Mg^{2+}@$B_{12}P_{12}$ (C-a model), and Ca^{2+}@$B_{12}P_{12}$ (D-a model) nanocages, the adsorption energy of PA on the surface of nanocage increased when the SEF strength was increased from 0 to 0.02 (a.u.) and then decreased when the SEF strength was increased from 0.02 to 0.075 (a.u.). Accordingly, it can be stated that in the A-a, C-a, and D-a models, the most appropriate strength for adsorbing PA on the surface of nanocage is 0.02 (a.u.). This result confirms that the SEF field in the gas phase is a suitable method for the adsorption and delivery of drugs in biological systems. In addition, the results related to the adsorption energy and electronic structures showed that pure $B_{12}P_{12}$ nanocage was not a good adsorbent or drug deliverer of PA. On the other hand, the results show that if Be^{2+}, Mg^{2+}, and Ca^{2+} ions are encapsulated inside the $B_{12}P_{12}$ nanocage, they will be good absorbents or deliverers of PA in biological systems. Interestingly, the water and ethanol solvent was found to play an important role in the biological processes by causing PA to separate from the $B_{12}P_{12}$ nanocage and delivering it to the target cells. This function of the water and ethanol solvent increased the therapeutic properties of PA. The $B_{12}P_{12}$ nanocages did not have a significant role in the drug treatment process.

Electronic Properties of PA/$B_{12}P_{12}$ Nanocage Complex

The quantum properties of the adsorption process. The structures of HOMO and LUMO orbitals for the occupied and unoccupied orbitals for all complexes [pristine $B_{12}P_{12}$, Be^{2+}@$B_{12}P_{12}$, Mg^{2+}@$B_{12}P_{12}$, and Ca^{2+}@$B_{12}P_{12}$] and all adsorption models [A-a to D-c] are presented in Fig. S2 and Fig. 3, respectively.

In all adsorption models, the highest density of the HOMO orbitals was concentrated on the surface of the nanocage. With the introduction of Be^{2+}, Mg^{2+}, and Ca^{2+} ions into the nanocage due to the ionic field, the highest density of HOMO orbitals expanded evenly around the nanocage. The surface of the nanocage, which is full of negative charges, is a favorable site for electrophilic attack. On the other hand, the highest density of the LUMO orbitals was concentrated on the surface of PA. It is noteworthy that density of HOMO orbitals expanded evenly around the nanocage. The surface of the nanocage, which is full of negative charges, is a favorable site for electrophilic attack.

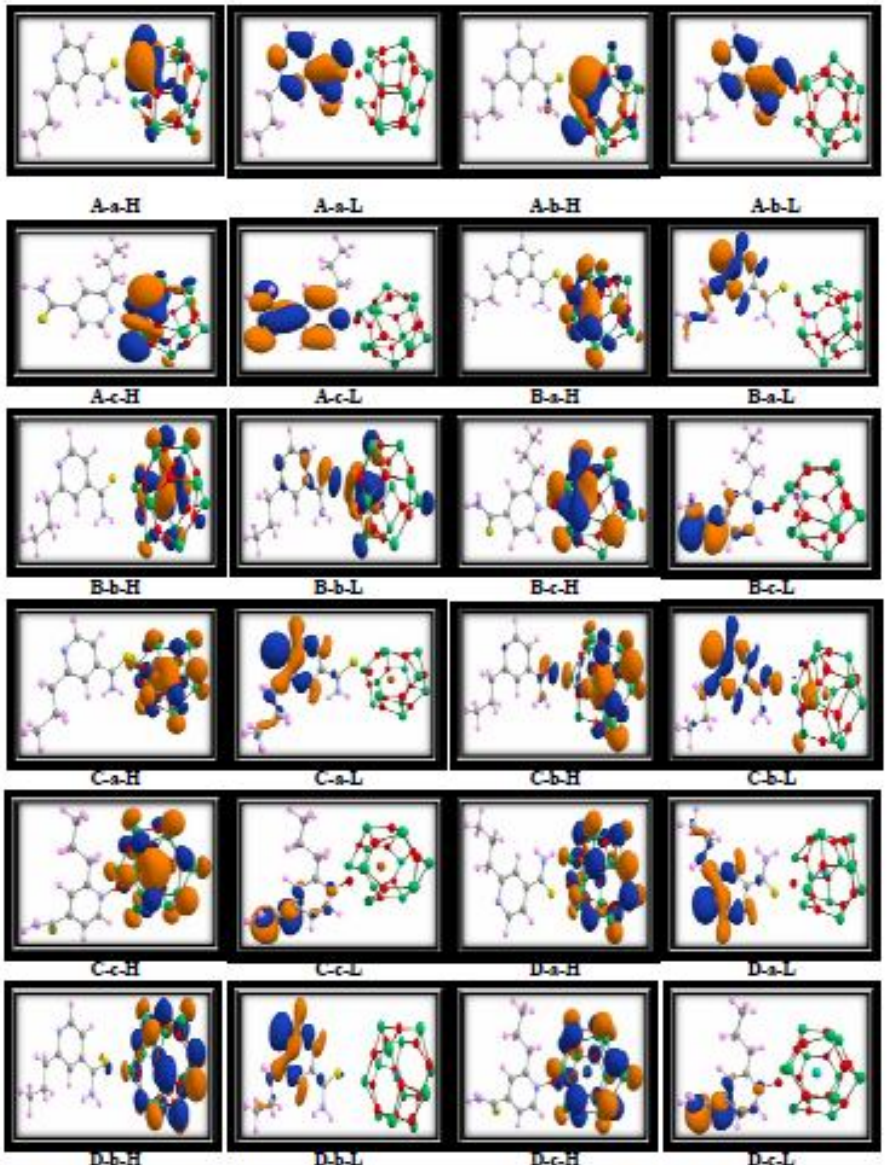

Fig. 3. The plots of HOMO and LUMO orbital structures for prothionamide (PA) adsorption on the surface of pristine and encapsulated Be^{2+}, Mg^{2+}, and Ca^{2+} ions into the $B_{12}P_{12}$ nanocage (A-a to D-c models).

On the other hand, the highest density of the LUMO orbitals was concentrated on the surface of PA. It is noteworthy that the density of LUMO on the surface of PA increased upon the introduction of Be^{2+}, Mg^{2+}, and Ca^{2+} ions; and as a result, PA became more vulnerable to nucleophilic attack. The highest density of the LUMO orbital was concentrated on the surface of the aromatic ring of PA, which enhances the therapeutic potential of PA. Quantum properties, such as energy gap, global hardness, chemical potential, electronegativity, and total charge transfer properties of systems were calculated from the HOMO and LUMO energies, and the results are presented in Table 3. The calculated results revealed that the energy gap and electron affinity of pristine $B_{12}P_{12}$ nanocage and PA were 3.94 and

3.91 (eV) and 6.60 and 14.85 (eV), respectively. By introducing Be^{2+} (B), Mg^{2+} (C), and Ca^{2+} (D) ions into the nanocage, the energy gap and global hardness of nanocage were significantly reduced compared to the pristine state; as a result, the conductivity and reactivity of nanocage increased. With the increase in the electron affinity and total charge transfer properties of $B_{12}P_{12}$ nanocage, the reactivity and tendency of the nanocage to absorb electrons increased significantly compared to the pristine state, resulting in an agreement with the HOMO orbital density.

It is worth noting that the encapsulated Be^{2+} ion had the greatest effect on the electrical behavior of nanocage and increased the conductivity and electron affinity of the nanocage, which plays an important role in the interaction between nanocage and PA adsorption. By adsorbing the PA on the surface of the $B_{12}P_{12}$ nanocage in the A-a to D-c adsorption models, the energy gap and global hardness of the system varied from 2.73 to 1.03 and from 1.97 to 0.51 eV, respectively. These results show that the conductivity of the $B_{12}P_{12}$ nanocage was significantly changed upon the adsorption of PA. This finding can facilitate the development and use of drug sensors in biological systems. The lowest energy gap and global hardness were related to the C-c model, but the conductivity and sensitivity of nanocage were higher in this model compared to other models.

($E_g = E_{LUMO} - E_{HOMO}$; $\eta = (E_{LUMO} - E_{HOMO})/2$; $\Delta N = -\mu/\eta$, $\omega = \mu^2/\eta$)) [50-54]

The electron affinity energy of all adsorption models varied between 7.60 and 100.26 (eV). The C-c model had the highest electron affinity; therefore, in this model, the nanocage had the greatest tendency to absorb electrons. This result is in agreement with the density of HOMO orbitals concentrated around the nanocage. To investigate the effects of the SEF on the electrical structure of the $PA/B_{12}P_{12}$ nanocage complex, the field strength of 0.005 to 0.04 (a.u.) was applied to the A-a, B-a, C-a, and D-a models, and the results are presented in Table 4. The comparison results showed that the HOMO, the LUMO, and the energy gap of the complex altered slightly in the absence of the SEF. This result confirms that the static field does not play a significant role in increasing the sensitivity of the sensor and the conductivity of the nanocage.

Density of states and partial density of states. The electronic density of state (DOS) and the partial density of state (PDOS) of $PA/B_{12}P_{12}$, $PA/Be^{2+}@B_{12}P_{12}$, $PA/Mg^{2+}@B_{12}P_{12}$, and $PA/Ca^{2+}@B_{12}P_{12}$ complexes, PA, and $B_{12}P_{12}$ nanocage were calculated within the range of -20 to 0 (eV) [53], and the results are shown in Fig. 4 and Fig. S4. Figure 4, which is related to the PDOS plot of PA and the $B_{12}P_{12}$ nanocage, shows that the number of electron transitions of $PA/B_{12}P_{12}$ complex (A-a, A-b, and A-c models) was greater in the HOMO region than in the LUMO region. However, with the encapsulation of Be^{2+}, Mg^{2+}, and Ca^{2+} ions into the nanocage, the number of transition states in the LUMO region increased significantly compared to the original state, which is a significant factor in reducing the energy gap. Secondly, two peaks appeared in the gap region upon the adsorption of PA on the surface of the $B_{12}P_{12}$ nanocage, which reflects a decrease in the energy gap of the nanocage. Interestingly, these peaks were much more evident in the C-c model than in other models. The energy gap of this model (*i.e.*, C-c model) was reduced to 1.03 (eV), and the electric conductivity of the nanocage, calculated using the $\sigma \propto e^{-Eg/2KT}$ [51-54], increased significantly compared to the original state. This finding can be used to turn PA into a sensitive sensor. A careful examination of the PDOS plots showed that the orbitals of PA contributed more to adsorption processes than those of $B_{12}P_{12}$ nanocage.

A comparison of the PDOS plots for all atoms in the $PA/B_{12}P_{12}$ complex showed that P atoms and H atoms in the A-a, A-b, and A-c models had the most and least contribution in the HOMO and LUMO regions, respectively. In the B-a and B-b models, the S and H atoms had the most and least contribution in the HOMO and LUMO regions, respectively, whereas in the B-c model, the N and S atoms had the most and least contribution in the HOMO and LUMO regions, respectively. In the C-a, C-b, and C-c models, the B, S, and P atoms had the most contribution in the HOMO and LUMO regions, respectively, while the H and N atoms had the least contribution in the HOMO and LUMO regions, respectively. In the D-a, D-b, and D-c models, the P, C, and H atoms had the most contribution in the HOMO and LUMO regions, respectively, while the H, P, and Ca atoms

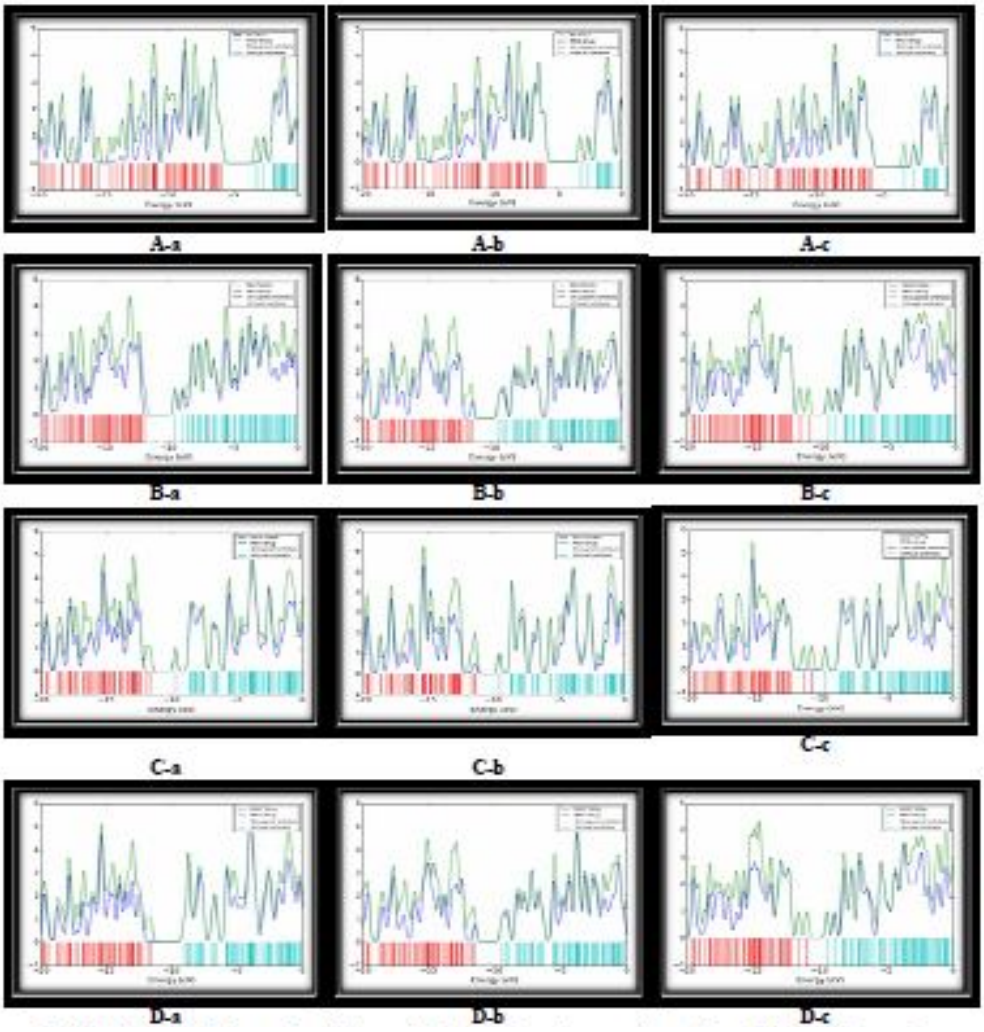

Fig. 4. The PDOS plots of prothionamide (PA) adsorption on the surface of the pristine and encapsulated Be^{2+}, Mg^{2+}, and Ca^{2+} ions into the $B_{12}P_{12}$ nanocage (A-a to D-c models).

had the least contribution in the HOMO and LUMO regions, respectively.

The reduced density gradient (RDG) scatter plots. The RDG scatter plots were used to investigate the non-covalent interactions between PA and $B_{12}P_{12}$, $Be^{2+}@B_{12}P_{12}$, $Mg^{2+}@B_{12}P_{12}$, and $Ca^{2+}@B_{12}P_{12}$ nanocages [55], and results are presented in Fig. 5. In the RDG scatter plots, the Y and X axes represent RDG and sign $(\lambda_2)\,\rho(r)$, respectively.

If the value of sign $(\lambda_2)\,\rho(r)$ is less than zero, it indicates a hydrogen or electrostatic bond between the two compounds. If it is equal to zero, it indicates a van der Waals bond, and if it is greater than zero, it indicates a nonbonding interaction.

As can be seen in Fig. 5, the type of bond between PA and the $B_{12}P_{12}$ nanocage in the A-a, A-b, and A-c models is van der Waals. However, in the encapsulated Be^{2+}, Mg^{2+}, and Ca^{2+} ions, the interaction between PA and $B_{12}P_{12}$ nanocage is more electrostatic due to the presence of a strong ionic field in the nanocage. It is noteworthy that this interaction was stronger in the presence of Be^{2+} ions than other ions, so the bond between PA and nanocage is stronger in this model compared to other models. This result

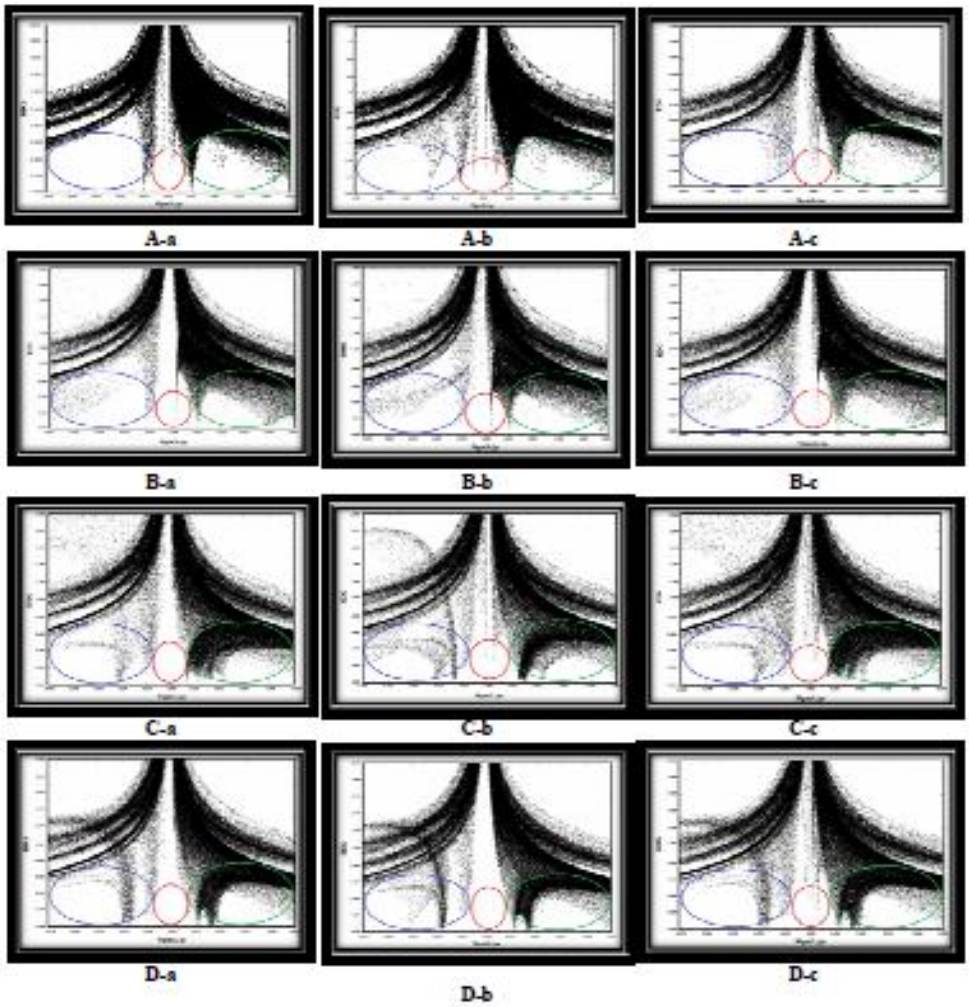

Fig. 5. The RDG plots of prothionamide (PA) adsorption on the surface of pristine and encapsulated Be^{2+}, Mg^{2+}, and Ca^{2+} ions into the $B_{12}P_{12}$ nanocage (A-a to D-c models).

is in agreement with the calculated adsorption energy and enthalpy of the system.

The UV-Vis and IR Spectra

The UV-Vis spectra of all adsorption models (A-a to D-c) are displayed in Fig. 6, and the electron density transitions that occurred in the UV-Vis spectra are listed in Table S3. The UV spectra of A-a, A-b, A-c, and B-a adsorption models show a relatively narrow peak in the 400 nm. However, in the B-b, B-c, C-a, C-b, C-c, D-a, D-b, and D-c adsorption models, a narrow peak can be seen in the range of 750 to 900 nm.

The UV-Vis spectra show that the absorption wavelength in the states [b] and [c] was longer than in the [a] state. The longest wavelength (λ_{max}) in the A-b (579.31 nm), B-b (574.35 nm), C-b (819.34 nm), and D-b (944.06 nm) models was related to electron transfer from (H→L), 0.59 (H-1→L+2), 0.88 (H→L), and 0.83 (H→L), respectively. In the A-c (503.90 nm), B-c (741.30 nm), C-c (672.06), and D-c (638.54 nm) models, the λ_{max} occurred at the 0.59 (H-9→L), 0.91 (H→L+1), 0.67 (H→L+2), and 0.45 (H-1→L) transition states, respectively (see Table S5). In the A models, the longest wavelength appeared at a 200 nm transition state.

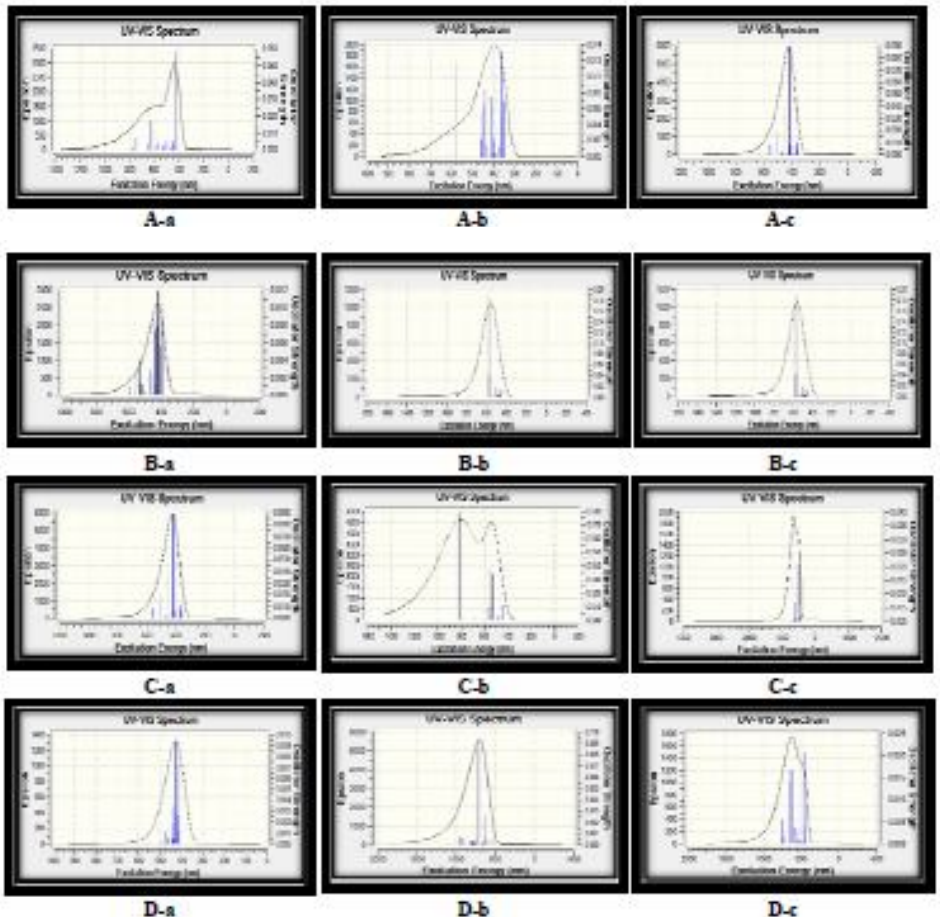

Fig. 6. The UV-Vis plots of prothionamide (PA) adsorption on the surface of pristine and encapsulated Be^{2+}, Mg^{2+}, and Ca^{2+} ions into the $B_{12}P_{12}$ nanocage (A-a to D-c models).

The infrared spectra of PA, $B_{12}P_{12}$, $Be^{2+}@B_{12}P_{12}$, $Mg^{2+}@B_{12}P_{12}$, $Ca^{2+}@B_{12}P_{12}$, and A-a to D-c adsorption models were calculated, and the results are illustrated in Fig. S1. According to the calculated results, the sharp peaks in PA occurred in 250, 850, 1250-1750, 3000-3250, 3550, and 3700 cm^{-1}, which are related to the stretching vibration of C=C, C-N, C=S, C-H, N-H, and C=N bonds, respectively. The band peak at around 900-1000 cm^{-1} is correlated to the stretching frequency of C-c bonds, and the band peaks at1350 and 1470 cm^{-1} can be assigned to the symmetric and asymmetric boding deformation of CH_2 bonds. In the pristine $B_{12}P_{12}$, $Be^{2+}@B_{12}P_{12}$, $Mg^{2+}@B_{12}P_{12}$, $Ca^{2+}@B_{12}P_{12}$ nanocages (see Fig. S1), a sharp peak can be seen at 900 cm^{-1}, which is correlated with the stretching vibration of B-P bonds of the nanocage.

The Atoms in Molecules (AIM) Theory

The AIM theory [56] was used to examine the interaction of PA with the pristine $B_{12}P_{12}$, $Be^{2+}@B_{12}P_{12}$, $Mg^{2+}@B_{12}P_{12}$, and $Ca^{2+}@B_{12}P_{12}$ nanocages [56]. Following the AIM theory, total electron density (ρ), Laplacian of electron densities ($\nabla^2\rho$), kinetic energy (G_{BCP}), total electronic energy (H_{BCP}), potential energy (V_{BCP}), and ellipticity (ε) were calculated for all adsorption models at the bond critical point (BCP), and the results are presented in Table 5. According to the results in Table 5, the values of $\nabla^2\rho$ and H_{BCP} for A-a, B-a, C-a, and D-a models from the S site of PA were negative. Based on the AIM theory, this result indicates a covalent bond between PA and the $B_{12}P_{12}$ nanocage. In the A-b, B-b, C-b, D-b, A-c, B-c, C-c, and D-c models, the values of $\nabla^2\rho$ and H_{BCP} were positive, which

Table 5. The Topological Parameters of PA/$B_{12}P_{12}$ Complex for A-a to D-c Models

	ρ	G(r)	H(r)	V(r)	ELF	LOL	ε	$\nabla^2\rho$
A-a	0.10	0.07	-0.09	-0.16	0.48	0.49	0.04	-0.08
B-a	0.14	0.07	-0.13	-0.20	0.69	0.60	0.05	-0.23
C-a	0.12	0.06	-0.11	-0.17	0.66	0.58	0.02	-0.20
D-a	0.12	0.06	-0.11	-0.17	0.66	0.58	0.02	-0.19
A-b	0.10	0.06	-0.09	-0.15	0.51	0.50	0.08	0.09
B-b	0.07	0.02	-0.02	-0.04	0.73	0.62	0.08	0.01
C-b	0.05	0.02	-0.01	-0.03	0.58	0.54	0.10	0.04
D-b	0.03	0.01	-0.01	-0.02	0.28	0.38	0.09	0.05
A-c	0.12	0.17	-0.09	-0.25	0.21	0.34	0.05	0.32
B-c	0.16	0.21	-0.13	-0.34	0.30	0.40	0.06	0.31
C-c	0.15	0.19	-0.12	-0.30	0.28	0.38	0.06	0.29
D-c	0.14	0.18	-0.11	-0.30	0.28	0.38	0.06	0.28

indicates that the type of bond between the NH_2 and N sites of PA was electrostatic. These results suggest that the binding of PA is stronger with nanocage than with other models. This property of PA can be used in drug delivery in biological systems. The results of these experimental calculations are in good agreement with thermodynamic calculations. The value of ε for all models was less than one, indicating that the bond between PA and the nanocage was a single bond or sigma.

Localized orbital locator (LOL) and Electron localization function (ELF) are used to determine the molecular regions that had the highest electron-pair density. According to the results in Table 5 and Fig. 6, while the values of LOL and ELF varied from 0.5 to 1 in the B-a, C-a, D-a, A-b, B-b, and C-b models, these values were less than 0.5 in other models. These results indicate that most electron charges were localized in the bonded and unbonded regions. Therefore, it can be stated that most electron charges were not localized in the bond region, which means the type of bond between PA and nanocage must have been electrostatic. This result is consistent with the results of the AIM theory.

CONCLUSIONS

In this research, the adsorption of PA from the S, NH_2, and N (pyridine) sites on the surface of pristine $B_{12}P_{12}$, $Be^{2+}@B_{12}P_{12}$, $Mg^{2+}@B_{12}P_{12}$, and $Ca^{2+}@$ $B_{12}P_{12}$ complexes were investigated in the absence and presence of a SEF. Comparison results showed that the adsorption energy and thermodynamic parameters were negative for all adsorption models and that all adsorption processes were exothermic and spontaneous. The calculated results showed that the dissociation of PA in the presence of water or ethanol solvent was more favorable at the [c] adsorption site than at the [a] and [b] adsorption sites of PA. Furthermore, the adsorption energy of PA on the surface of the $B_{12}P_{12}$ nanocage increased from 0 to 0.02 (a.u.) SEF strength and then decreased from 0.02 to 0.075 (a.u.) SEF strength.

In all adsorbed models, the energy gap and global hardness of the system varied from 2.73 to 1.03 and from 1.97 to 0.51 (eV), respectively. These results show that the conductivity and sensitivity of the nanocage significantly changed upon the adsorption of PA. This result can facilitate the development of drug sensors in biological systems. The UV-Vis spectra of A-a, A-b, A-c, and B-a adsorption models showed a relatively narrow peak at 400 nm. However, in the B-b, B-c, C-a, C-b, C-c, D-a, D-b, and D-c adsorption models, a narrow peak was observed at the range of 750 to 900 nm. The AIM, LOL, ELF, and NBO results revealed that the type of bond between the NH_2 and N sites of PA and the nanocage was electrostatic. These results confirm that the binding of PA was stronger with nanocage than with other models, making PA a promising

candidate for use in drug delivery in biological systems.

ACKNOWLEDGMENTS

The authors would like to thank the Information Technology Center of Malayer University for providing the necessary software and data used to carry out this research.

Supplementary Data

Tables S1-S5 and Figs. S1-S5 are provided in supplementary data.

REFERENCES

[1] Paine, R. T.; Narula, C. K., Synthetic routes To boron nitride, *Chem. Rev.* **1990**, *90*, 73-91. doi.org/10.1021/cr00099a004.

[2] Wu, H. S.; Zhang, F. Q.; Xu, X. H.; Zhang, C. J.; Jiao, H., Geometric and energetic aspects of aluminum nitride cages, *J. Phys. Chem. A,* **2003**, *107*, 204-209. doi.org/10.1021/jp027300i.

[3] Zhu, H. Y.; Schmalz, T. G.; Klein, D. J., Alternant boron nitride cages: A theoretical study, *Int. J. Quantum Chem.* **1997**, *63*, 393-401. doi.org/10.1002/(SICI)1097-461.

[4] Wang, Q.; Sun, Q.; Jena, P.; Kawazoe, Y., Potential of AlN nanostructures as hydrogenStorage materials, *ACS Nano,* **2009**, *3*, 621-626. doi.org/10.1021/nn800815e.

[5] Amani, J.; Khoshroo, A.; Rahimi-Nasrabadi, M., Electrochemical immunosensor for the breast cancer marker CA 15-3 based on the catalytic activity of a CuS/reduced graphene oxide nanocomposite towards the electrooxidation of catechol, *Microchim. Acta.* **2018**, *185*, 79. doi.org/10.1007/s00604-017-2532-5.

[6] Khoshroo, A.; Hosseinzadeh, L.; Sobhani-Nasab, A.; Rahimi-Nasrabadi, M.; Ehrlich, H., Development of electrochemical sensor for sensitive determination of oxazepam based on silver-platinum core-shell nanoparticles supported on grapheme. *J. Electroanal. Chem.* **2018**, *823*, 61-66. DOI: 10.1016/ j.jelechem.2018.05.030.

[7] Beheshtian, J.; Kamfiroozi, M.; Bagheri, Z.; Ahmadi, A., $B_{12}N_{12}$ nano-cage as potential sensor for NO_2 detection, *Chin. J. Chem. Phys.* **2012**, *25*, 60-64. doi.org/10.1088/1674-0068/25/01/60-64.

[8] Amani, J.; Maleki, M.; Khoshroo, A.; Sobhani-Nasab, A.; Rahimi-Nasrabadi, M., An electrochemical immunosensor based on polyp-phenylenediamine and graphene nanocomposite for detection of neuron-specific enolase via electrochemically amplified detection. *Anal. Biochem.* **2018**, *548*, 53-59. DOI: 10.1016/j.ab.2018.02.024.

[9] Aghazadeh, M.; Barmi, A. A. M.; Hosseinifard, M., Nanoparticulates $Zr(OH)_4$ and ZrO_2 prepared by low-temperature cathodic electrodeposition, *Mater. Lett.* **2012**, *73*, 28-31. DOI: 10.1016/j.matlet.2011.12.118.

[10] Beheshtian, J.; Kamfiroozi, M.; Bagheri, Z.; Ahmadi, A., Computational study of CO and NO adsorption on magnesium oxide nanotubes, *Physica E,* **2011**, *44*, 546-549. DOI: 10.1016/j.physe.2011.09.016.

[11] Rad, A. S.; Ayub, K., Adsorption of thiophene on the surfaces of $X_{12}Y_{12}$ (X = Al, B, AndY = N,P) nanocages; A Dft study, *J. Mol. Liq.* **2017**, *238*, 303-309. DOI: 10.1016/j.molliq.2017.05.020.

[12] Ayub, K., Binding affinity and permeation of $X_{12}Y_{12}$ nanocages for heliumand Neo, *J. Mol. Liq.* **2017**, *244*, 124-134. DOI: 10.1016/j.molliq.2017.08.118.

[13] Strout, D. L., Structure and stability of boron nitrides: Isomers of $B_{12}N_{12}$. *J. Phys. Chem. A,* **2000**, *104*, 3364-3366. doi.org/10.1021/jp994129a.

[14] Wang, R.; Zhang, D.; Liu, C., Theoretical prediction of a novel inorganic fullerene-like family of silicon-carbon materials, *Chem. Phys. Lett.* **2005**, *411*, 333-338. DOI: 10.1016/J.CPLETT.2005.06.055.

[15] Paine, R.; Narula, C., Synthetic routes to boron nitride. *Chem. Rev.* **1990**, *90*, 73-91. doi.org/10.1021/cr00099a004.

[16] Wu, H. -S.; Zhang, F. -Q.; Xu, X. -H.; Zhang, C. -J.; Jiao, H., Geometric and energetic aspects of aluminum nitride cages. *J. Phys. Chem. A.* **2003**, *107*, 204-209. doi.org/10.1021/jp027300i.

[17] Zhu, H. -Y.; Schmalz, T. G.; Klein, D. J., Alternant boron nitride cages: A theoretical study. *Int. J. Quantum. Chem.* **1997**, *63*, 393-401. doi.org/10.1002/ (SICI) 1097-461.

[18] Wang, Q.; Sun, Q.; Jena, P.; Kawazoe, Y., Potential of AlN nanostructures as hydrogen storage materials.

Acs. Nano. **2009**, *3*, 621-626. doi.org/10.1021/nn800815e.

[19] Naderi, H. R.; Sobhani-Nasab, A.; Rahimi-Nasrabadi, M.; Ganjali, M. R., Decoration of nitrogen-doped reduced graphene oxide with cobalt tungstate nanoparticles for use in high-performance supercapacitors, *Appl. Surf. Sci.* **2017**, *423*, 1025-1034. DOI: 10.1016/j.apsusc.2017.06.239.

[20] Beheshtian, J.; Bagheri, Z.; Kamfiroozi, M.; Ahmadi, A., A comparative study on the $B_{12}N_{12}$, $Al_{12}N_{12}$, $B_{12}P_{12}$, and $Al_{12}P_{12}$ fullerene-like cages, *J. Mol. Model.* **2012**, *18*, 2653-2658. DOI: 10.1007/s00894-011-1286-y.

[21] Oku, T.; Nishiwaki, A.; Narita, I., Formation and atomic structure of $B_{12}N_{12}$ nanocage clusters studied by mass spectrometry and cluster calculation. *Sci. Technol. Adv. Mater.* **2004**, *5*, 635-638. doi.org/10.1016/j.stam.2004.03.017.

[22] Oku, T.; Kuno, M.; Kitahara, H.; Narita, I., Formation, atomic structures and properties of boron nitride and carbon nanocage fullerene materials. *Int. J. Inorg. Mater.* **2001**, *3*, 597-612. DOI: 10.1016/S1466-6049(01)00169-6.

[23] Rad, A. S.; Ayub, K., A comparative density functional theory study of guanine chemisorption on $Al_{12}N_{12}$, $Al_{12}P_{12}$, $B_{12}N_{12}$, And $B_{12}P_{12}$ Nano-Cages, *J. Alloys. Comp.* **2016**, *672*, 161-169. DOI: 10.1016/j.jallcom.2016.02.139.

[24] Rad, A. S.; Bagheri Novir, S.; Mohseni, S.; Ramezani, N.; Mirabai, A., A DFT study of O_2 and Cl_2 adsorption onto $Al_{12}N_{12}$ fullerene-like nanocluster, *Heteroat. Chem.* **2017**, *28*, 21396. doi.org/10.1002/hc.21396.

[25] Rad, A. S., Comparison of $X_{12}Y_{12}$ (X = Al, B and Y = N, P) fullerene-like nanoclusters toward adsorption of dimethyl ether, *J. Theor. Comput. Chem.* **2018**, *17*, 1850013. doi.org/10.1142/S021963361850013X.

[26] Yong, Y.; Liu, K.; Song, B.; He, P.; Wang, P.; Li, H., Coalescence of bnnn fullerenes: A new pathway to produce boron nitride nanotubes with small diameter, *Phys. Lett. A*, **2012**, *376*, 1465-1467. doi.org/10.1142/S021963361850013X.

[27] Wu, H.; Fan, X.; Kuo, J. L., Metal-free hydrogenation reaction on carbon doped boron nitride fullerene: A DFT study on the kinetic issue, *Int. J. Hydrog. Energy,* **2012**, *37*, 14336-14342. DOI: 10.1016/j.ijhydene.2012.07.081.

[28] Beheshtian, J.; Ahmadipeyghan, A.; Bagheri, Z., Quantum chemical study of fluorinated AlN nano-cage, *Appl. Surf. Sci.* **2012**, *259*, 631-636. doi.org/10.1016/j.apsusc.2012.07.088.

[29] Beheshtian, J.; Bagheri, Z.; Kamfiroozi, M.; Ahmadi, A., A comparative study on the $B_{12}N_{12}$, $Al_{12}N_{12}$, $B_{12}P_{12}$ and $Al_{12}P_{12}$ fullerene-like cages, *J. Mol. Model,* **2012**, *18*, 2653-2658. DOI: 10.1007/s00894-011-1286-y.

[30] Rad, A. S., Studyonthe surface interaction of furan with $X_{12}Y_{12}$ (X = B, Al, And Y = N, P) semiconductors: DFT calculations, *Heteroatom Chem.* **2016**, *27*, 316-322. DOI: 10.1002/hc.21342.

[31] Ferreira, V.; Alves, H., Boron phosphide as the buffer-layer for the epitaxial III-nitride growth: A theoretical study, *J. Crys. Grow.* **2008**, *310*, 3973-3978. DOI: 10.1016/J.JCRYSGRO.2008.06.039.

[32] Beheshtian, J.; Peyghan, A. A.; Bagheri, Z., Selective function of $Al_{12}N_{12}$ nanocagetowards No and Co molecules, *Comput. Mater. Sci.* **2012**, *62*, 71-74. DOI: 10.1016/j.commatsci.2012.05.041.

[33] Beheshtian, J.; Bagheri, Z.; Kamfiroozi, M.; Ahmadi, A., Toxic Co detection by $B_{12}N_{12}$ nanocage, *Microelectron. J.* **2011**, *42*, 1400-1403. DOI: 10.1016/j.mejo.2011.10.010.

[34] Beheshtian, J.; Kamfiroozi, M.; Bagheri, Z.; Ahmadi, A., Theoretical study of hydrogen adsorption on the $B_{12}P_{12}$ fullerene-like nanocage, *Comput. Mater. Sci,* **2012**, *54*, 115-118. DOI: 10.1016/ J.COMMATSCI.2011.09.039.

[35] Soltani, A.; Baei, M. T.; Ramezani Taghartapeh, M.; Tazikeh Lemeski, E.; Shojaee, S., Phenol interaction with different nano-cages withand without an electric field: A DFT study, *Struct. Chem.* **2015**, *26*, 685-693. doi.org/10.1007/s11224-014-0504-5.

[36] Padash, R.; Rahimi-Nasrabadi, M.; Rad, A. S.; Sobhani-Nasab, A.; Jesionowski, T.; Ehrlich, H., A comparative computational investigation of phosgene adsorptionOn $(XY)_{12}$ (X = Al, B and Y = N, P) nanocages: DFT investigations, *J. Cluster Sci.* **2019**,

30, 203-218. doi.org/10.1007/s10876-018-1479-y.

[37] Sajida Munsif, A.; Maria, A.; Saima Khan, A.; Asghar Ali, A.; Amjad Gilani, M.; Iqbal, J.; Ralf, C. D.; Ludwig, E. F.; Ayub, K., Remarkable nonlinear optical response of alkali metal doped aluminum phosphide and boron phosphide nanocages, *J. Mol. Liq*. **2018**, *271*, 51-64. DOI: 10.1016/ j.molliq.2018.08.121.

[38] Rad, A. S.; Ayub, K., How can nickel decoration affect H_2 adsorption on $B_{12}P_{12}$ nano-heterostructures? *J. Mol. Liq*. **2018**, *255*, 168-175. doi:10.1016/j.molliq.2018.01.149.

[39] Kosar, N.; Asgar, M.; Ayub, K.; Mahmood, T., Halides encapsulation in aluminum/boron phosphide nanocages: An effective strategy for high cell voltage in Na-ion battery, *Mater. Sci. In Semiconductor Proc.* **2019**, *97*, 71-79. DOI: 10.1016/j.mssp.2019.03.011.

[40] Ayub, K., Transportation of hydrogen atom and moleculethrough $X_{12}Y_{12}$ nano-cages, *Inter. J. Hydrogen Energy*. **2017**, *42*, 11439- 1451. DOI: 10.1016/j.ijhydene.2017.02.202.

[41] Beheshtian, J.; Kamfiroozi, M.; Bagheri, Z.; Ahmadi, A., Theoretical study of hydrogen adsorption on the $B_{12}P_{12}$ fullerene-like nanocage, *Comp. Mate Sci.* **2012**, *54*, 115-118. DOI: 10.1016/ J.COMMATSCI.2011.09.039

[42] Razavi, R.; Najafi, M., Potential of $Si_{14}Ge_{14}$ and $B_{14}P_{14}$ nanocages as electrodes of metal-ion batteries: A theoretical investigation, *J. Solid State Electrochem.* **2019**, *23*, 759-769. DOI: 10.1007/s00894-018-04176-3

[43] Rad, A. S.; Aghaie, S. M.; Poralijan, V.; Peyravi, M.; Mirzaei, M., Application of pristine and Ni-decorated $B_{12}P_{12}$ nano-clusters as superior media for acetylene and ethylene adsorption: DFT calculations, *Comp. Theor. Chem*. **2017**, *1109*, 1-9. DOI: 10.1016/j.comptc.2017.03.030

[44] Hojatkashaniorienta, L., Adsorption behavior of Co on pristine and doped $B_{12}P_{12}$ nanocage: A DFT study, *J. Chem.* **2015**, *31*, 2087-2097. doi.org/10.13005/ojc/310429

[45] Kian, M.; Tazikeh-Lemeski, E., $B_{12}Y_{12}$ (Y: N, P) Fullerene-like cages for exemestane-delivery; molecular modeling investigation, *J. Mol. Str.* **2020**, *1217*, 128455. doi.org/10.1016/j.molstruc.2020.128455.

[46] Najafi, M., The SH functionalized $B_{24}N_{24}$ and $B_{24}P_{24}$ nanocages as potential sensor for oxygen difluoride (OF_2) detection in the gas phase and methanol, *Vacuum*, **2017**, *135*, 18-21. DOI: 10.1016/j.vacuum.2016.10.023.

[47] Soltani, A.; Baei, M. T.; Mirarab, M.; Sheikhi, M.; Tazikeh Lemeski, E.,The electronic and structural properties of BN And BP nano-cages interacting with Ocn_: A DFT study, *J. Phys. Chem. Solids*. **2014**, *75*, 1099-1105. doi.org/10.1016/j.jpcs.2014.05.005.

[48] Rezaei-Sameti, M.; Shiravand, E., The thermodynamic, quantum, AIM and NBO study of the interaction of pyrazinamide drug with the pristine and transition metal-doped $B_{12}P_{12}$, *Adsorption*, **2020**, *26*, 955-970. DOI: 10.1007/s10450-019-00181-8.

[49] Frisch, M. J., *et al*., Gaussian 09, Revision D.01, **2009**.

[50] Rezaei-Sameti, M.; Abdoli, S. K., The capability of the pristine and (Sc, Ti) doped $Be_{12}O_{12}$ nanocagetodetect and adsorb of mercaptopyridine molecule: A first principle study. *J. Mol. Str.* **2020**, *1205*, 127593-13. DOI: 10.1016/ j.molstruc.2019.127593.

[51] Rezaei-Sameti, M.; Zarei, P., NBO, AIM, HOMO-LUMO and thermodynamic investigationof the nitrate ion adsorption on the surface of pristine, Al and Ga doped BNNTs: A DFT study, *Adsorption*,**2018**, *24*(8), 757-767. DOI: 10.1007/s10450-018-9977-7.

[52] Rakhshi, M.; Mohsennia, M.; Rasa, H.; Rezaei Sameti, M., First-principle study of ammonia molecules adsorption on boron nitride nanotubes in presence and absence of static electric field and ion field, *Vacuum*, **2018**, *155*, 456-464. doi.org/10.1016/j.vacuum.2018.06.047.

[53] Rezaei-Sameti, M.; Zanganeh, F., A computational study of adsorption H_2S gas on the surface of the pristine, Al&P-doped armchair and zigzag BNNTs, *J. Sulfur. Chem.* **2017**, 38, 384–400. doi.org/10.1080/17415993.2017.1313255.

[54] Rezaei-Sameti, M.; Behbahani, H. J., Interaction of HCN molecule with the pristine and Al, S and Al & S doped beryllium oxide nanotube: A computational

study, *Phys. Chem. Res.* **2018**, *6*, 31-43. DOI: 10.22036/PCR.2017.89007.1388.

[55] Sun, Y. T.; Huang, P. Y.; Lin, C. H.; Lee, K. R.; Lee, M. T., Studying antibiotic-membrane interactions *via* X-ray diffraction and fluorescence microscopy, *BioPhys. J.* **2015**, *110*, 414-418. DOI: 10.1016/j.fob.2015.06.006.

[56] Bader, R. W. F., Atoms in Molecules: A Quantum Theory. Oxford University Press, Oxford, **1994**.